

A Finite Difference Approximate Fractional-Order Gradient Operator for Improving Image Classification Performance

Nuh ALPASLAN

*Bingol University, Department of Computer Engineering, Bingol 12000
TURKEY (e-mail: nalpaslan@bingol.edu.tr).*

Abstract: This study presents a finite difference fractional order gradient operator to enhance CoHOG feature extraction for image classification problems. A finite difference Euler approximation of fractional-order derivative (FOD) filter structure is used for the fractional-order gradient calculations for derivative orders around the value of one. The proposed gradient operator is employed for CoHOG feature extraction and performance improvements obtained in image classification are demonstrated over six image sets containing about 15000 images. It is observed that roughly 5% improvement is possible in average correct classification percentage (CCO) at the fractional gradient order of 0.4 when compared to average correct classification percentage of the conventional gradient with the integer order of 1.0. In the case of proper fraction-orders selection particular to dataset, classification accuracy improvements can be obtained up to 14.8% depending on dataset.

Keywords: CoHOG, fractional-order derivative, gradient operator, image classification.

1. INTRODUCTION

Feature extraction is a fundamental task in many image processing applications such as texture classification et al., 2012), emotion recognition (Senechal et al., 2012), handwritten character recognition (Sundaram and Ramakrishnan, 2013), fish species classification (Rodrigues et al., 2014), blood vessel detection (Fathi and Naghsh-Nilchi, 2011) and human action recognition (Marín-Jiménez et al., 2012). Feature extraction aims to decrease the amount of resources needed for describing a large set of data accurately. Feature extraction methods perform two essential tasks: it transforms input parameter vectors into feature vectors as an early processing and thus reduces the dimensionality and complexity of data (Wang and Paliwal, 2003; Fathi and Naghsh-Nilchi, 2011; He et al., 2012; Marín-Jiménez et al., 2012; Senechal et al., 2012; Sundaram and Ramakrishnan, 2013; Rodrigues et al., 2014).

In image classification problems, generation of feature vectors from image data is considered as an early processing task and the generated feature vectors directly feeds to input of classifiers. Hence, a well-defined feature extraction algorithm makes the image classification process more effective and robust (Wang and Paliwal, 2003). Due to the fact that visual appearance is difficult to model due to complicating factors, such as high variability of texture, illumination variance of surfaces, cluttered background, pose...etc., appearance based algorithms need powerful classifiers using robust features (Liu et al., 2011). The widely used feature descriptors in image processing are edge and orientation information.

To improve object identification performance in images, gradient-based features were developed which are edge orientation histogram (EOH) (Gerónimo et al., no date),

histograms of oriented gradients (HOG) (Dalal and Triggs, 2005; Talu et al., 2013), co-occurrence HOG (CoHOG) (Watanabe et al., 2009), multilevel edge energy features (Maji et al., 2008), shapelets (Sabzmeydani and Mori, 2007), and edge density (Phung and Bouzerdoum, 2007). Both EOH and HOG methods distribute the gradients into several orientation bins. EOH features are the ratio between the summed gradient magnitudes of two bins for a given rectangular region. The HOG method encapsulates alterations in the magnitude and orientation of contrast over a grid of small image patches. Especially, HOG features show satisfactory performance in recognition of different object types including natural objects as well as artificial objects (Watanabe et al., 2009; Ren et al., 2010). Gradient-based features present two benefits: one is the robustness against illumination variance because gradient orientations of local regions do not alter much with illumination variance (Watanabe et al., 2009). The other is the robustness against deformations because slight shifts and affine deformations do not make significant changes in the histogram (Watanabe et al., 2009). However, histogram based features have limited discriminative power because spatial information is not well represented by histograms. For the solution of this problem, CoHOG (co-occurrence histograms of oriented gradients), an extension of HOG to represent the spatial relationship between gradient orientations, has been proposed and its effectiveness for medical image analysis (Talu et al., 2013), pedestrian detection (Sabzmeydani and Mori, 2007), human detection (Phung and Bouzerdoum, 2007) and cat face detection (Kozakaya et al., 2009; Do and Kijak, 2012), object detection (Ren et al., 2010; Xu et al., 2012) has been demonstrated.

Discussion on a fractional-order derivative (FOD) traced back in the seventeenth century (G.W. Leibnitz, no date).

Some approximate definitions for the calculation of FOD were proposed by Grünwald-Letnikov, Riemann-Liouville and Caputo (Oldham and Spanier, 1974; I. Podlubny, 1999). Renewed interest in fractional-order calculus due to the recent successful applications in engineering and applied science (Ross, 1975; Sabatier et al., 2007; Gutiérrez et al., 2010) is the motivation of our study. In recent years, there is also growing interest for fractional-order methods in image processing problems (Gan and Yang, 2010; Gao et al., 2011; Gao et al., 2012; Jalab and Ibrahim, 2013). Several works have been proposed for the use of fractional-order mask and gradient definitions in edge detection (Mathieu et al., 2003), image registration (Melbourne et al., 2012) and image enhancement (Yang et al., 2011): Fractional-order differentiation was used for enhanced image registration via MR data (Melbourne et al., 2012). Yan et al. demonstrated an application proving fractional calculus in image processing in a widespread zone (Yang et al., 2011). A multiscale mask based on Riemann-Liouville fractional differential was proposed for texture enhancement (Qing, 2012). Another texture enhancement application was presented by using fractional differential masks in (Jalab and Ibrahim, 2013). A fractional calculus operator based on piecewise quadratic interpolation equation was also presented for image enhancement (Gao et al., 2011). Multiscale texture enhancement was proposed by using fractional directional differentiation (Gao et al., 2012). Fractional differentiation (FD) for edge detection was shown to exhibit better edge detection performance for noisy image (Mathieu et al., 2003; Tian et al., 2013, 2014; Bento et al., 2017). Iris localization application used fractional differential edge detectors (Lu and Xie, 2008). Object classification based on fractional HoG features were discussed (Liu and Shen, 2011). Investigation of fractional order differentiation and its applications in digital image processing is proposed in (He et al., 2015). A new medical image enhancement method is presented by taking the merits of fractional differential and directional derivative in (Guan et al., 2018). Fractional order differentiation, fractional order gradient magnitude, and difference image information into the well-known local Chan-Vese model is used for modeling the local information to incorporate image gradient in (Chen et al., 2019).

In the current study, we aim to investigate impacts of fractional-order finite difference gradient operation on image classification performance of CoHOG descriptors. We use Euler finite difference approximate formulation based on Euler discretization for FOD operator performing the derivative orders around the values of one. Main advantage of the finite difference fractional-order derivative (FDFOD) formulation is that it provides a simplified and low computational complexity solution for approximate calculation of fractional-order derivative in operating ranges. This approximate formulation of FOD is particularly proposed for image processing applications where computational complexity is a key issue for practical realization. In fact, it can be seen as very simplified version of Grünwald-Letnikov discrete derivative to approximate FOD around the values of zero in case of the fractional orders around one. For the derivative

order one, it simplifies well-known backward finite difference approximation formula of the discrete first order derivatives.

We formulated a Euler finite difference based approximate fractional-order gradient (FDFOG) operator for two dimensional spatial data (images) and used it in the gradient orientation calculations in CoHOG. The classification performance of CoHOG feature descriptor with the FDFOG was tested for various fractional derivative orders in the image classification problem and classification performances are reported. Tests were performed by seven test image sets composed of totally 15000 images. Consequently, the FDFOG classification results present a possibility of a higher classification performance compared to conventional discrete gradient operators based on backward finite difference approximation of the first derivative.

Organization of the paper is as follows: Section 2 was devoted for the theoretical background for image classification by using CoHOG. The finite difference fractional-order gradient formulation was presented in the Section 3. In section 4, the classification performance of the CoHOG feature descriptor using the FDFOG was demonstrated by experimental tests performed on totally seven image sets. The conclusions are summarized in the section 5.

2. THEORETICAL BACKGROUND

2.1. CoHOG Feature Extraction

CoHOG is an effective gray level feature descriptor based on gradient orientations (Watanabe et al., 2009). The CoHOG methods yield co-occurrence matrices which express the distribution of gradient orientations for a given offset. This process is shown in Fig. 1. The combinations of neighbor gradient orientations provide reliable features for object recognition in images, and therefore it is very beneficial for image classification problems.

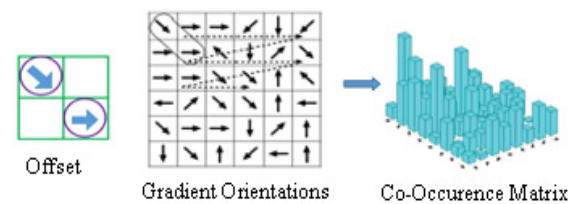


Fig. 1. A co-occurrence matrix of gradient orientations. For a given offset gradient orientations are calculated on image regions.

$$\theta(i, j) = \tan^{-1} \frac{u(i, j)}{v(i, j)} \quad (1)$$

$$C_{i,j} = \sum_{p=0}^{n-1} \sum_{q=0}^{m-1} \begin{cases} 1 & \text{if } \theta(p, q) = i \text{ and } \theta(p+x, q+y) = j \\ 0 & \text{otherwise} \end{cases} \quad (2)$$

where the matrix θ represents gradient orientations and the parameters x and y represent vertical and horizontal offset values. Where u and v are the vertical and the horizontal components of gradient vectors, respectively. The overview of CoHOG calculation is represented in Fig. 2.

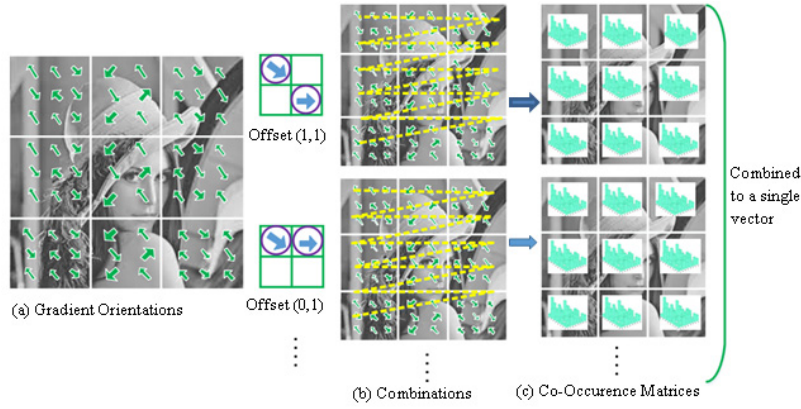


Fig. 2. Overview of CoHOG calculation.

The image is divided into tiled regions, co-occurrence matrices are calculated for ten different offsets $\{(0,1), (0,2), (1,1), (1,2), (2,1), (1,0), (2,0), (1,-1), (1,-2), (2,-1)\}$ and combined into a single vector. Firstly, gradient orientations (θ) are calculated by Eq. (1) as shown in Fig. 2 (a) and orientation angles in the range $[0,2\pi)$ are quantized into eight labels, which are $\{1,2,3,4,5,6,7,8\}$. Each label stands for an orientation for each pixel. For instance, orientation angle in the range of $(\pi/4, \pi/2]$ is labeled by the number “2”. The indices (i, j) represent pixel positions in image matrix denoted by $I(i, j)$. Secondly, the co-occurrence matrix C is obtained by gradient orientations of $n \times m$ image according to Eq. (2) as shown in Fig. 2 (b). A pixel-pair can be represented by an offset, which express the spatial relationship between two points. Ten different offsets $\{(0,1), (0,2), (1,1), (1,2), (2,1), (1,0), (2,0), (1,-1), (1,-2), (2,-1)\}$ were used in the experiments. The offsets are shown in Fig. 3. The co-occurrence matrix conveys information related with the local textures by using short-range offsets and the global textures by using long-range offsets (Watanabe et al., 2009). By using both short range and long range offsets, the co-occurrence matrices can express more detail on shapes. In addition, relative location and orientation are considered with each neighboring pixel, respectively, which is more precise to describe the shapes. The co-occurrence matrices are computed for each region with all offsets as shown in Fig 2 (c). Finally, the components of all the co-occurrence matrices are concatenated into a single vector.

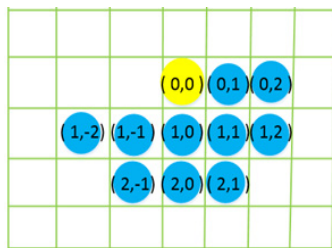


Fig. 3. Offsets for co-occurrence matrices. The 10 blue circles are pairs for the offsets.

From one tiled region, CoHOG obtains 10 co-occurrence matrices. Each co-occurrence matrix has 8×8 components.

Therefore the dimension of CoHOG is $m \times n \times d^2$, where d is the number of gradient orientation bins, m is the number of tiled regions and n is the number of offsets.

2.2. Image Classification Process

A block diagram of how to perform image classification by using CoHOG is illustrated in Fig. 4. Gradient orientations (θ) are calculated from spatial gradient of image intensity matrix (I). Then, the CoHOG schema generates the co-occurrence matrices (C) forming the features that are used by neural network classifier to recognize objects in images.

Artificial neural network (ANN), which was inspired by the biological nervous systems, is a machine learning tool, and it essentially resembles the learning from experiences. Many research works demonstrated that ANN can provide robust classification performance (Chen and Folly, 2018; Hsu et al., 2018; Jafari-Marandi et al., 2018; Xiang et al., 2018). Some successful classification applications of ANN are bankruptcy prediction, breast cancer diagnosis (Jafari-Marandi et al., 2018), rainfall prediction (Xiang et al., 2018) and Wind Power Forecasting (Chen and Folly, 2018). The main advantage of ANN in classification problems is its ability to detect complex nonlinear relationships between dependent and independent variables. We used feed forward back propagation neural network (BPNN) for classification of extracted features. Feed forward BPNN is a well-known ANN model, and it is very effective in classification problems. It contains three neuron layer groups which are input, hidden and output layers. In the training stage, the training data is fed into the inputs. Each neuron in the input layer, hidden layer and output layer calculate their output values. Then, actual output values are compared with the target output values at ANN output. The errors between these outputs are calculated and propagated back to hidden layer in order to update the weight of neurons in a way that error iteratively descends through training process. The training process of ANN continues until the error reaches acceptable levels. After the training stage, test inputs are fed into the input layer, and the feed forward network will generate results from trained network (Hsu et al., 2018). In ANN simulations, the 10-fold cross validation method was used for reliable performance assessment.

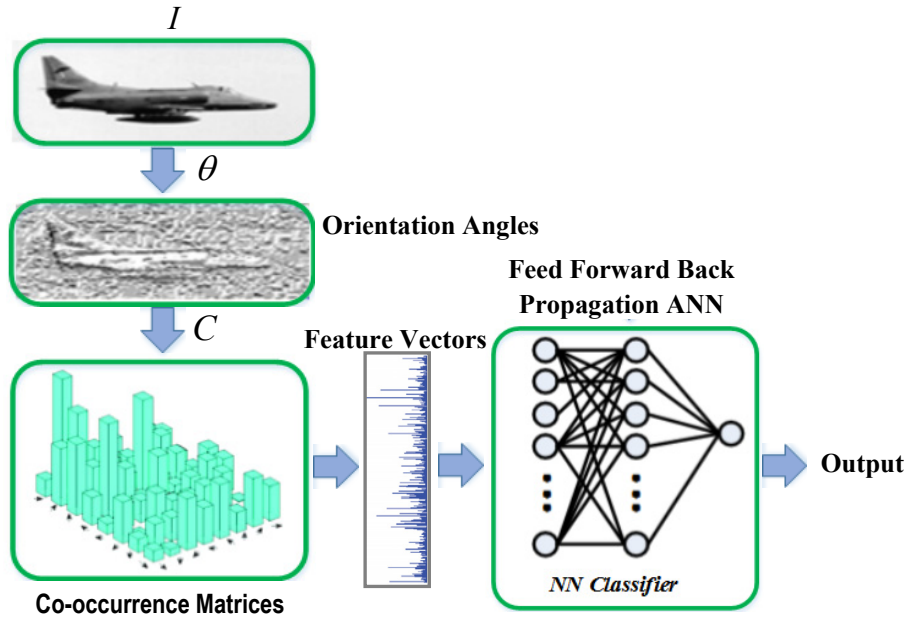


Fig. 4. Block diagram of image classification task based on CoHOG.

Object recognition performance not only depends on classification capabilities of the ANN classifiers but also depends on discriminative capability of obtained features. In the current study, we modify gradient operator by FOD techniques to improve discriminative features of CoHOG feature vectors. This modification allows adjustment of fractional-order gradient operator and contribute to finding a non-integer derivative order that can provide better classification performance than the classical gradient operator. In other words, FOD makes gradient operators tunable for accomplishment of better classification performance. The following sections demonstrate classification performance improvements obtained by fractional gradient order.

3. FINITE DIFFERENCE FRACTIONAL-ORDER GRADIENT APPROXIMATION FOR IMAGE DATA

Discrete-time filter structure were used to realize fractional-order derivative operators in practice (Lubich, 1986; Chen et al., 2009; Karci, 2013; Nosrati and Shafiee, 2018; Zarei and Tabatabaei, 2018). One of the well-known filter structures for discrete implementation of derivatives is Euler approximation, suggesting generating function of derivative operator $s \approx \frac{1}{T}(1-z^{-1})$, and fractional-order derivative is expressed in discrete filter form $s^\alpha \approx \frac{1}{T^\alpha}(1-z^{-1})^\alpha$ according to Euler approximation [43,44] and its filter form can be written by:

$$F(z) = \frac{1}{T^\alpha} (1-z^{-1})^\alpha X(z) \quad (3)$$

where parameter T is sampling period and the parameter α denotes the fractional-order. For $\alpha > 0$ values, FOD filter with Euler approximation performs an approximate α -order derivative of time series signal $x(n)$. When equation (3) is

rearranged, Euler approximation for the FOD can be written as,

$$F(z) = \frac{1}{T^\alpha} (X(z)^{1/\alpha} - Z^{-1}X(z)^{1/\alpha})^\alpha \quad (4)$$

This study needs fractional gradient operation the α order values of around the value of one. The case of $\alpha = 1$ refers to the first derivative and results in a conventional gradient operation based on finite difference Euler approximation. When the α is close to one ($\alpha \approx 1$) and considering z^{-1} delay element as the sampling time T , Euler discrete filter form of FOD filter approximates the following finite difference (FD) implementation of FDFOD in the discrete time domain (n):

$$\frac{d^\alpha f(n)}{dn^\alpha} \cong \frac{1}{h^\alpha} \left(x(n)^{\frac{1}{\alpha}} - x(n-T)^{\frac{1}{\alpha}} \right)^\alpha \quad (5)$$

As a natural result of being an approximate solution, the results of FDFOD filter can diverge from results of exact fractional-order derivatives. A similar approach for the definition of fractional order derivative was discussed by Karci and a fractional order derivative operator was expressed based on the limit definition of first derivative operator (Karci, 2013).

Fig. 5 presents a comparison of results of FDFOD filter and the exact fractional-order derivative of polynomials, defined as $D^\alpha f_n = \sum_{i=0}^n a_i \frac{\Gamma(i+1)}{\Gamma(i-\alpha+1)} x^{i-\alpha}$. Results of theoretic and the discrete approximate solutions are consistent for small values $x \in [2, -2]$ and this is acceptable for image processing because fractional derivative is calculated in a local window with small sizes.

Gradient operator is based on directional derivatives and yields a gradient vector \vec{G} over scalar fields. Fractional-order

gradient (\bar{G}^α) of a scalar field $f: R^n \rightarrow R$ is commonly expressed depending on the fractional-order derivatives as,

$$\bar{G}^\alpha = \nabla^\alpha f(x_1, x_2, \dots, x_n) = \sum_{k=1}^n \frac{d^\alpha f}{dx_k^\alpha} \bar{e}_{x_k} \quad (6)$$

where, \bar{e}_{x_k} is unit vector in the direction of dimension x_k . Image data defines a two-dimensional scalar field of intensity distribution represented by the matrix I . By considering Eq. (4) for α -order derivatives, the finite difference based fractional-order gradient of image matrix can be calculated by,

$$u^\alpha = \frac{\partial^\alpha I}{\partial i^\alpha} \cong \frac{1}{h_i^\alpha} \left(I(i, j)^\alpha - I(i - h_i, j)^\alpha \right) \quad (7)$$

$$\theta^\alpha(i, j) = \tan^{-1} \left(\frac{\left(I(i, j)^\alpha - I(i - h_i, j)^\alpha \right)^\alpha}{\left(I(i, j)^\alpha - I(i, j - h_j)^\alpha \right)^\alpha} \right) \quad (12)$$

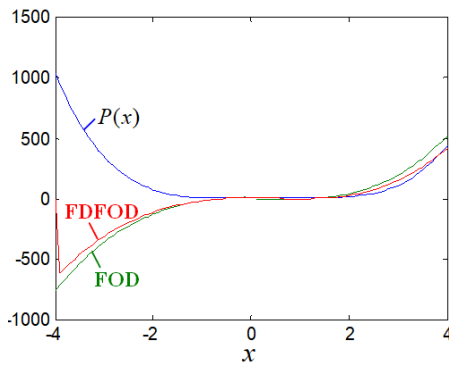


Fig. 5. Results of FDFOG ($T = 0.1, \alpha = 1.2$) and exact fractional-order derivative (FOD) fractional order derivative of the polynomial, $P(x) = 3x^4 - 5x^3 - 2x^2 + 5x + 5$.

When working on image matrixes, $h_i = h_j = 1$ are regularly configured for discrete derivative operation. In fact, the

$$v^\alpha = \frac{\partial^\alpha I}{\partial j^\alpha} \cong \frac{1}{h_j^\alpha} \left(I(i, j)^\alpha - I(i, j - h_j)^\alpha \right) \quad (8)$$

$$\bar{G}_I^\alpha(i, j) = \nabla^\alpha I(i, j) = u^\alpha i + v^\alpha j, \quad (9)$$

where, h_i and h_j are spatial sampling length of image data I in the vertical directions (i) and horizontal directions (j), respectively. The u^α and v^α are FDFOG vectors. Magnitude and angle of \bar{G}_I^α were expressed as:

$$|\bar{G}_I^\alpha(i, j)| = \left(u^{2\alpha} + v^{2\alpha} \right)^{\frac{1}{2}} \quad (10)$$

$$\theta(\bar{G}_I^\alpha(i, j)) = \tan^{-1}(u^\alpha / v^\alpha) \quad (11)$$

orientation information derived from $\theta(\bar{G}_I^\alpha)$ given by Eq. (11) can be rewritten as in Eq. (12).

The orientation angles of pixels were shifted π rad in order to limit angles between $[0, 2\pi)$.

$$\theta_I(i, j) = \theta^\alpha(i, j) + \pi \quad (13)$$

For a better classification performance, feature descriptors should reduce unnecessary information from the raw data and keep information associated to desired features. Fig. 6 shows orientation images calculated by FDFOG for various α . The figure reveals that α parameter has an effect on the value diversity in orientation data. The information theory suggests that the amount of information can be assessed by the Shannon entropy. As known, entropy rate of information was defined as $\log_2 m$ for m -level quantization of a zero-order source model in information theory (Shannon, 1949; Balian, 2004; Alagoz and Alisoy, 2014).

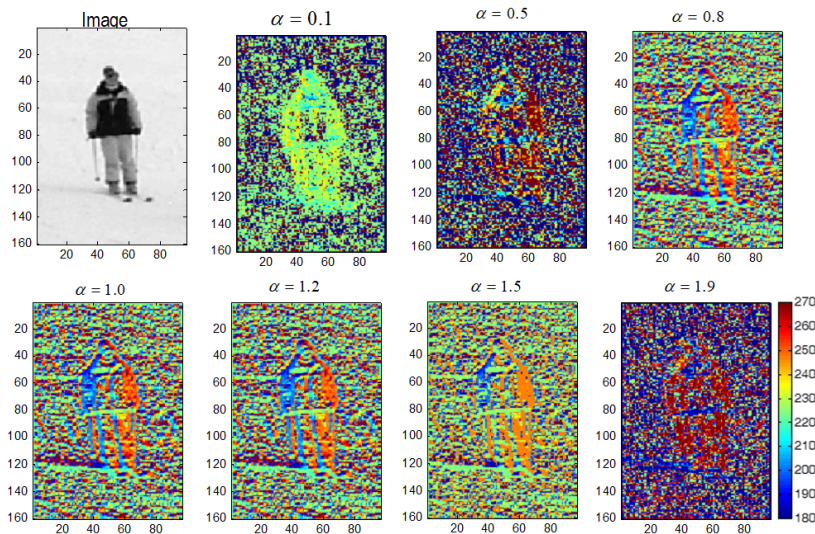


Fig. 6. A positive person image from Inria dataset and the fractional order gradient orientation images with FDFOG for various α .

We observed that the entropy rate of gradient orientation data decreases as values of α diverge from the value of one. This effect is apparent in Fig. 7. Fig. 7 illustrates 8-level quantization of orientation angles (Labeling) for the person positive image, which contains a person in the image, and the person negative image, which does not contain any person in image. For $\alpha = 1.0$, eight labels $\{1,2,3,4,5,6,7,8\}$ were used to quantize gradient orientations and the entropy rate is $\log_2 8 = 3$. However, for $\alpha = 0.4$, three labels $\{4,5,6\}$ in eight label set are enough for quantization of gradient orientations and therefore the entropy rate of quantized gradient orientations is $\log_2 3 = 1.58$. This shows that gradient orientation data for $\alpha = 1.0$ presents a higher entropy compared to the case of $\alpha = 0.4$. This decrease of entropy in orientation image data purifies the feature description, particularly for the object region and this effect can improve the classification performance. Because, it provides richer co-occurrence matrices for neural network classifier. High entropy in orientation images causes rather flat co-occurrence matrices with very low values and it is indeed a factor reducing the performance of neural classifiers. On the other hand, if entropy rate is too low, it may cause the loss of useful feature information and therefore, this situation can also reduce classification performance. So, there is a need

for finding a suitable α -order that can provide enhanced overall classification performance in all datasets. Our simulation results show that $\alpha = 0.4$ provides the best overall performance for seven datasets.

4. APPLICATION OF FINITE DIFFERENCE FRACTIONAL-ORDER GRADIENT IN COHOG FOR IMAGE CLASSIFICATION

This section discusses the effects of derivative order and compares image classification test results.

We used six datasets: INRIA, Caltech4, Caltech5, Caltech Cars, Light and Caltech Airplanes. Section 4.1 briefly explains each test dataset used in our experiments. In Section 4.2, we present computer experiment results and the corresponding performance evaluations.

4.1 Datasets

Following datasets was used in computer experiments.

Inria: This dataset is used to classify an image on whether it contains a person or not. 2416 normalized images for positive samples, and 1218 images for negative samples were used in training process. In test process, a total of 1208 images resized to 64×128 (Dalal, 2006).

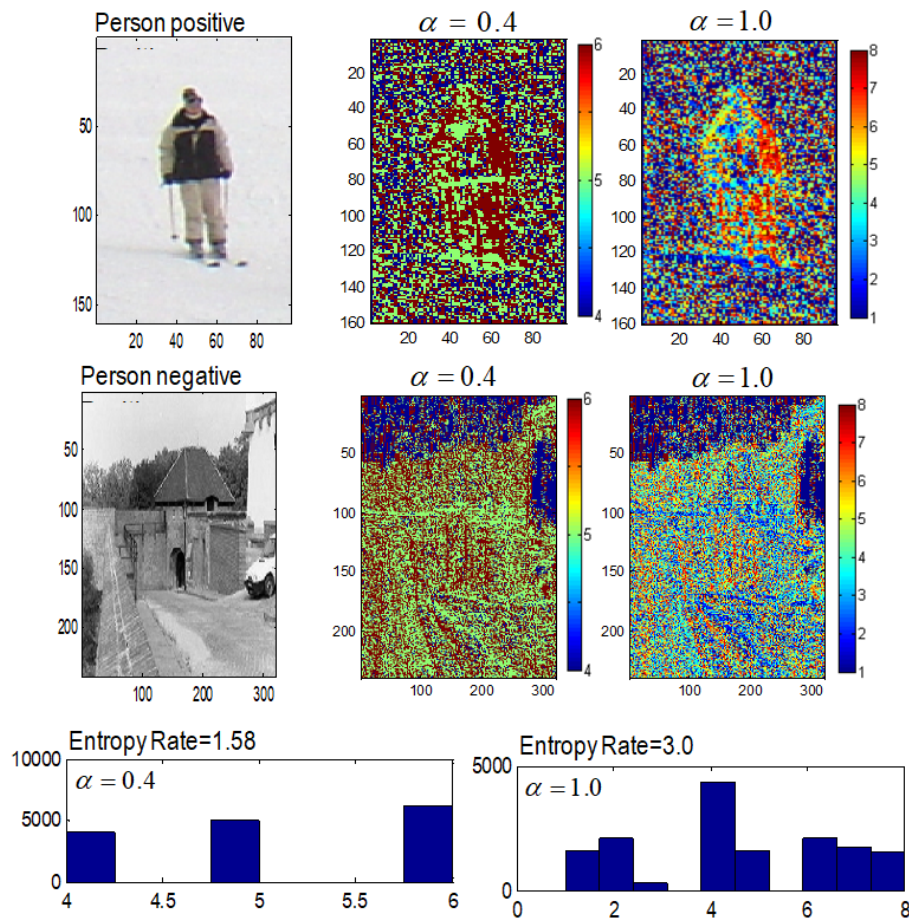


Fig. 7. Person positive and person negative images from Inria dataset and the 8 level quantized fractional order gradient orientation images (orientation labeled images) with FDFOG for $\alpha = 0.4$ (The best overall performance) and $\alpha = 1.0$ (The conventional gradient performance). Bar graphs at the bottom show histogram of 8 level quantized orientation of person positive images.

Caltech256: This dataset consists of images from 256 object categories. The size of each image is roughly 300×200 pixels. For each independent experiment, different image categories were used. For example, to build a dataset with four classes, the images in the categories such as motorbikes, leopards, bonsai and watch were gathered and this dataset was renamed as Caltech4. In the same manner, Caltech5 (motorbikes, faces, toaster, binocular, cars rear) dataset was formed. In training process, 1155 images from Caltech4, 1607 images from Caltech5 dataset were used. In test process, 200 images from Caltech4 and 208 images from Caltech5 were classified (Griffin et al., 2007).

Light: This dataset consists of 2400 light microscope images of liver cell, which contains the tissues healthy or not. In training process, 864 images for positive samples, and 1296 images for negative samples were used. Training images have 256×192 size. In test process, a total of 240 images were used (Griffin et al., 2007).

4.2. Experimental Results

Computer experiments for image classification were conducted by an Intel Core i7-3520M processor, 2.9GHz with 8GB of RAM running 64-bit Windows operating system. The method was implemented by using Matlab. In computer simulations, 10 different offsets $\{(0,1), (0,2), (1,1), (1,2), (2,1), (1,0), (2,0), (1,-1), (1,-2), (2,-1)\}$ were used. The dimensions of CoHOG were equal to 640 for per tiled region (10 (number of offsets) $\times 8^2$ (number of orientation bin)). A back propagation neural network was used to implement classifier. Input of neural network classifier is fed by co-occurrence matrix in vector form as in Figs. 2 and 3. Output of the classifier yields classification results coded as 1 for positive and 0 for negative. The neural network composed of 1280 inputs, 640 hidden layer neurons and relevant numbers of output neurons depending on number of classes (5 neurons for Caltech5, 4 neurons for Caltech4 and 1 neuron for Inria, Caltech Cars, Caltech Airplanes and Light datasets). Image classification tests were repeated only once for each dataset.

Image classification tests for α , changing from 0 to 2 with 0.1 steps, were performed on six datasets {Inria, Caltech4 (Calt4), Caltech5(Calt5), Caltech Cars (CaltCar), Caltech Airplanes (CaltPlane), Light} containing about 15000 images totally. Fig. 8 shows correct classification performance (accuracy) of datasets for varying α order.

A common way to evaluate experimental image classification results is to use the accuracy (p_c). The accuracy is the proportion of true results (both true positives and true negatives) to all results in the test population and gives us a statistical data for evaluation of the correct classification performance.

In order to figure out the α value, which exhibits the highest overall classification performance for all datasets, the average of correct classification percentages were drawn versus α in Fig. 9 (a). This figure shows that the best average

classification performances for all datasets were obtained for $\alpha = 0.2$ and $\alpha = 0.4$ with average correct classification percentages of $Avg(p_c(\alpha = 0.2)) = 90.1$ and $Avg(p_c(\alpha = 0.4)) = 91.1$. Conventional gradient operator ($\alpha = 1.0$) presents an average correct classification percentage of 86.1 ($Avg(p_c(\alpha = 1.0)) = 86.1$). So, the FDFOG with $\alpha = 0.2$ and $\alpha = 0.4$ exhibited a better image classification performance compared to the conventional gradient operator ($\alpha = 1.0$) that is indeed implements well-known Euler backward difference approximation formula.

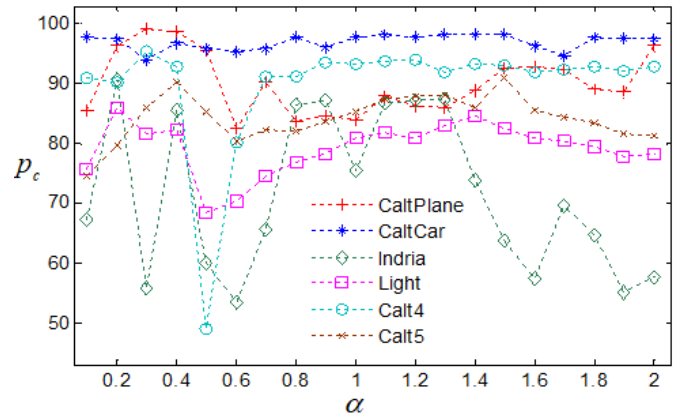


Fig. 8. Percentage of correct classification (accuracy- p_c) for 6 datasets depending on the fractional order α .

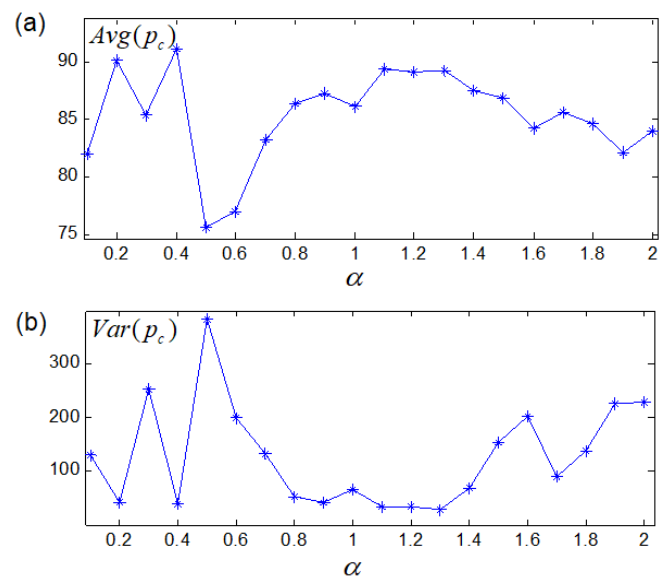


Fig. 9. (a) Average of correct classification percentages (p_c) (b) Variance of correct classification percentages (p_c).

Fig. 9 (b) shows the variance of correct classification percentages in order to see the consistency of overall performance improvement in datasets. Lower variance indicates that average correct classification percentages are consistent among datasets. The figure reveals that the classification performances obtained for $\alpha = 0.2$ and $\alpha = 0.4$ are also consistent among six datasets ($Var(p_c(\alpha = 0.2)) = 43$ and $Var(p_c(\alpha = 0.4)) = 40$). One can conclude that $\alpha = 0.2$ and $\alpha = 0.4$ can preserve their

efficiency from a dataset to another in the different six datasets, compared to the performance of conventional gradient ($\alpha = 1.0$), ($Var(p_c(\alpha = 1.0)) = 66$).

In application, the use of a fixed value of α , such as $\alpha = 0.2$ or $\alpha = 0.4$, provides about 5% in average improvement in the classification performance. If the dataset oriented variable α selection is used in the orientation calculation, better performance per dataset is obtainable as shown in Table 1. The correct classification percentages in the case of the best α selection are compared with percentages of $\alpha = 0.4$ and $\alpha = 1.0$ in the table. Variable α selection per dataset improves about 6.8% in overall. This is about 2.2% higher than the performance of the fixed $\alpha = 0.4$.

Table 1 also reveals that a better classification performance is mostly possible for the low values of α such as 0.2 and 0.4. One of the reasons of this effect is the lower entropy in gradient orientation images for $\alpha = 0.2$ and $\alpha = 0.4$ (Entropy: $\log_2 3 = 1.58$) as seen in Fig. 7. Because, possibility of repeating quantized orientations pattern (repeating label pattern) increases in the case of low entropy, this provides richer co-occurrence matrices to feed neural network classifier.

When $\alpha = 1$, FDFOD calculation (Equation (4)) performs a well-known backward finite difference linear approximation,

that is commonly used for the discrete first derivative. When $\alpha \neq 1$, it performs backward finite difference operation in a nonlinear fashion. However, use of FDFOG method results in too much increase in computational complexity only for gradient vector calculations. Because, it needs three additional power operations for an α -order derivative as

$$\text{seen in the term of } \left(x(n)^{\frac{1}{\alpha}} - x(n-T)^{\frac{1}{\alpha}} \right)^{\alpha}$$

to the conventional backward finite difference approximation of the discrete first derivative, using the term of $(x(n) - x(n-T))$. In our tests, image classification time per 134×204 pixels image is about 0.131094 seconds by using FDFOG and 0.130973 seconds by using conventional gradient with backward finite difference Euler approximation. This results in 0.0092% (about 0.000121 second) increase in image classification for an image with 134×204 size. In practice, this increase in computation time is negligible.

Table 1. Variable α selection per dataset and performance improvements.

	<i>Inria</i>	<i>Caltech4</i>	<i>Caltech5</i>	<i>Caltech Cars</i>	<i>Caltech Airplanes</i>	<i>Light</i>	<i>Overall p_c</i>
<i>Best α and p_c</i>	$\alpha = 0.2$ 90.2%	$\alpha = 0.3$ 95.3%	$\alpha = 0.4$ 90.2%	$\alpha = 1.3$ 98.3%	$\alpha = 0.3$ 99.1%	$\alpha = 0.2$ 86.1%	93.2%
<i>p_c for $\alpha = 1.0$</i>	75.4%	93.2%	85.4%	97.8%	85.4%	81.0%	86.3%
<i>p_c for $\alpha = 0.4$</i>	85.4%	92.8%	90.2%	96.8%	98.6%	82.4%	91%
<i>Improvement rates of the best α according to $\alpha = 1.0$</i>	14.8%	2.1%	4.8%	0.5%	13.7%	5.1%	6.8%

Fig. 10 shows ROC curves for Light and Caltech Airplanes datasets. The ROC curves validate that FDFOG for $\alpha = 0.4$ provides improved image classification performance

compared to conventional CoHOG ($\alpha = 1.0$). Table 2 summarizes some important performance parameters and confirms performance improvement provided by $\alpha = 0.4$.

Table 2. Sensitivity, specificity, precision, fall-out and F1 scores obtained for Light and Caltech Airplanes datasets at $\alpha = 0.4$ and $\alpha = 1.0$

	<i>Light dataset</i>		<i>Caltech Airplanes dataset</i>	
	$\alpha = 0.4$	$\alpha = 1.0$	$\alpha = 0.4$	$\alpha = 1.0$
<i>Sensitivity (Recall)</i>	0.85	0.65	0.98	0.96
<i>Specificity</i>	0.88	0.87	0.98	0.95
<i>Precision</i>	0.82	0.77	0.98	0.95
<i>Fall-out</i>	0.11	0.12	0.01	0.04
<i>F1 Score</i>	0.83	0.71	0.98	0.96

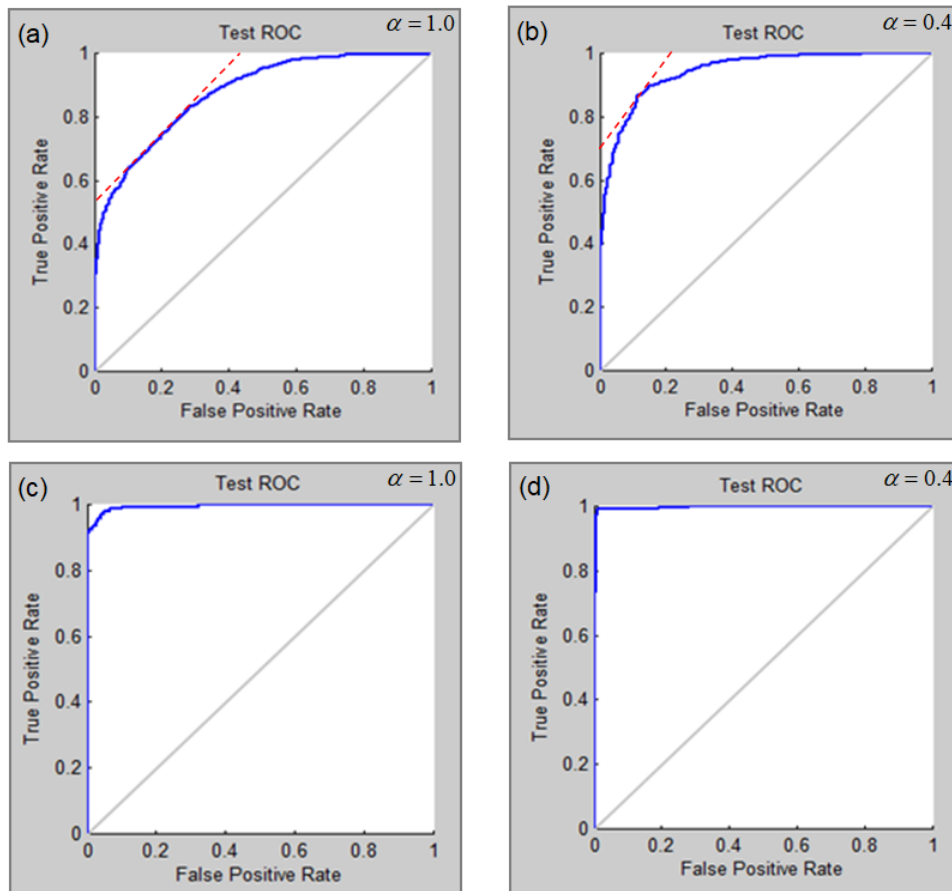


Fig. 10. ROC curve generated for Light and Caltech Airplanes datasets: (a) Light dataset for $\alpha = 1.0$; (b) Light dataset for $\alpha = 0.4$; (c) Caltech Airplanes dataset for $\alpha = 1.0$; (d) Caltech Airplanes dataset for $\alpha = 0.4$

5. CONCLUSIONS

This paper presents FDFOG operator for images and demonstrates its advantages for image classification with CoHOG descriptor. We observed that FDFOG operator can provide 5% improvement in average for the fixed α selection ($\alpha = 0.4$) and 6.8% improvement in average in the case of the dataset oriented variable α selection. The computer experiments conducted for 15000 images reveals that it is possible to improve the performance of image classification accuracy by using FDFOG which increase average accuracy from 86% (using conventional gradient operator) to over 90% (using proposed gradient operator) in this study.

FDFOG provides a low computational complexity, finite difference nonlinear approximation for α -order gradient operation around zero value and the order one. When $\alpha = 1$, it performs well-known backward finite difference linear approximation for the discrete first derivative. When $\alpha \neq 1$, it, indeed, performs a nonlinear backward finite difference operation. We demonstrated that FDFOG with $\alpha \neq 1$ can improve CoHOG performance in image classification problems.

As a consequence, this study confirms the reports that fractional calculus can be useful to improve the performance of image processing methods.

6. REFERENCES

- Alagoz, B. B. and Alisoy, H. Z. (2014) 'Sequence Partitioning and Compression Rate', *Balkan Journal of Electrical and Computer Engineering*. Balkan Journal of Electrical & Computer Engineering (BAJECE), 2(1).
- Balian, R. (2004) 'Entropy, a Protean Concept', *Poincaré Seminar 2003*. Birkhäuser Basel, pp. 119–144.
- Bento, T. et al., (2017) 'Fractional Order Image Processing of Medical Images', *Journal of Applied Nonlinear Dynamics*. L&H Scientific Publishing, LLC, 6(2), pp. 181–191. doi: 10.5890/jand.2017.06.005.
- Chen, B. et al., (2019) 'A fractional order derivative based active contour model for inhomogeneous image segmentation', *Applied Mathematical Modelling*. Elsevier Inc., 65, pp. 120–136. doi: 10.1016/j.apm.2018.08.009.
- Chen, Q. and Folly, K. A. (2018) 'Wind Power Forecasting', *IFAC-PapersOnLine*. Elsevier, 51(28), pp. 414–419. doi: 10.1016/j.ifacol.2018.11.738.
- Chen, Y., Petras, I. and Xue, D. (2009) 'Fractional order control - A tutorial', *2009 American Control Conference*. IEEE. doi: 10.1109/acc.2009.5160719.
- Dalal, N. (2006) *Finding People in Images and Videos*.

- Grenoble Institute of Technology.
- Dalal, N. and Triggs, B. (2005) 'Histograms of Oriented Gradients for Human Detection', in *IEEE Computer Society Conference on Computer Vision and Pattern Recognition (CVPR'05)*. Institute of Electrical and Electronics Engineers (IEEE), pp. 886–893.
- Do, T.-T. and Kijak, E. (2012) 'Face recognition using Co-occurrence Histograms of Oriented Gradients', *IEEE International Conference on Acoustics, Speech and Signal Processing (ICASSP)*. IEEE.
- Fathi, A. and Naghsh-Nilchi, A. R. (2011) 'General rotation-invariant local binary patterns operator with application to blood vessel detection in retinal images', *Pattern Analysis and Applications*. Springer Nature, 17(1), pp. 69–81.
- G.W. Leibnitz (no date) 'Letter from hanover, germany, september 30, 1695 to g. a. l'hospital', *Leibnizen Mathematische Schriften*. Olms Verlag Hildesheim, Germany, 1962, First published in 1849.
- Gan, Z. and Yang, H. (2010) 'Texture enhancement through multiscale mask based on RL fractional differential', *2010 International Conference on Information, Networking and Automation (ICINA)*. IEEE. doi: 10.1109/icina.2010.5636376.
- Gao, C. et al., (2011) 'Image enhancement based on improved fractional differentiation', *Journal of Computational Information Systems*, 7(1), pp. 257–264.
- Gao, C., Zhou, J. and Zhang, W. (2012) 'Fractional Directional Differentiation and Its Application for Multiscale Texture Enhancement', *Mathematical Problems in Engineering*. Hindawi Limited, 2012, pp. 1–26. doi: 10.1155/2012/325785.
- Gerónimo, D. et al., (no date) 'Haar Wavelets and Edge Orientation Histograms for On-Board Pedestrian Detection', *Pattern Recognition and Image Analysis*. Springer Berlin Heidelberg, pp. 418–425.
- Griffin, G., Holub, A. and Perona, P. (2007) *Caltech-256 Object Category Dataset*. California Institute of Technology. Available at: <https://authors.library.caltech.edu/7694/> (Accessed: 21 February 2018).
- Guan, J. et al., (2018) 'Medical Image Enhancement Method Based on the Fractional Order Derivative and the Directional Derivative', *International Journal of Pattern Recognition and Artificial Intelligence*. World Scientific Publishing Co. Pte Ltd, 32(3). doi: 10.1142/S021800141857001X.
- Gutiérrez, R. E., Rosário, J. M. and Tenreiro Machado, J. (2010) 'Fractional Order Calculus: Basic Concepts and Engineering Applications', *Mathematical Problems in Engineering*. Hindawi Limited, pp. 1–19.
- He, N. et al., (2015) 'An improved fractional-order differentiation model for image denoising', *Signal Processing*. Elsevier, 112, pp. 180–188. doi: 10.1016/j.sigpro.2014.08.025.
- He, Y., Sang, N. and Gao, C. (2012) 'Multi-structure local binary patterns for texture classification', *Pattern Analysis and Applications*. Springer Nature, 16(4), pp. 595–607.
- Hsu, Y.-Y. et al., (2018) 'Two-Stage Artificial Neural Network Model for Short-Term Load Forecasting', *IFAC-PapersOnLine*. Elsevier, 51(28), pp. 678–683.
- I. Podlubny (1999) *Fractional Differential Equations: Mathematics in Science and Engineering*, New York and Tokyo Academic Press. doi: 10.17694/bajece.52354.
- Jafari-Marandi, R. et al., (2018) 'An optimum ANN-based breast cancer diagnosis: Bridging gaps between ANN learning and decision-making goals', *Applied Soft Computing*. Elsevier, 72, pp. 108–120.
- Jalab, H. A. and Ibrahim, R. W. (2013) 'Texture Enhancement for Medical Images Based on Fractional Differential Masks', *Discrete Dynamics in Nature and Society*. Hindawi Limited, pp. 1–10.
- Karci, A. (2013) 'A New Approach for Fractional Order Derivative and Its Applications', *Universal Journal of Engineering Science*. Horizon Research Publishing, 1(3), pp. 110–117.
- Kozakaya, T. et al., (2009) 'Cat face detection with two heterogeneous features', *16th IEEE International Conference on Image Processing (ICIP)*. IEEE.
- Liu, Y. and Shen, X. D. (2011) 'Object Classification Based on Fractional HoG Features', *Applied Mechanics and Materials*. Trans Tech Publications, 65, pp. 491–496.
- Liu, Yang, Liu, Yan and Chan, K. C. C. (2011) 'Tensor-based locally maximum margin classifier for image and video classification', *Computer Vision and Image Understanding*. Elsevier BV, 115(3), pp. 300–309.
- Lu, J. and Xie, M. (2008) 'Use fractional calculus in iris localization', *2008 International Conference on Communications, Circuits and Systems*. IEEE. doi: 10.1109/iccacs.2008.4657925.
- Lubich, C. (1986) 'Discretized Fractional Calculus', *SIAM Journal on Mathematical Analysis*. Society for Industrial & Applied Mathematics (SIAM), 17(3), pp. 704–719.
- Maji, S., Berg, A. C. and Malik, J. (2008) 'Classification using intersection kernel support vector machines is efficient', *IEEE Conference on Computer Vision and Pattern Recognition*. IEEE.
- Marín-Jiménez, M. J., Pérez de la Blanca, N. and Mendoza, M. Á. (2012) 'Human action recognition from simple feature pooling', *Pattern Analysis and Applications*. Springer Nature, 17(1), pp. 17–36.
- Mathieu, B. et al., (2003) 'Fractional differentiation for edge detection', *Signal Processing*. Elsevier BV, 83(11), pp. 2421–2432.
- Melbourne, A. et al., (2012) 'Using fractional gradient information in non-rigid image registration: application to breast MRI', *Medical Imaging 2012: Image Processing*. SPIE.
- Nosrati, K. and Shafiee, M. (2018) 'Kalman filtering for discrete-time linear fractional-order singular systems', *IET Control Theory and Applications*. Institution of Engineering and Technology, 12(9), pp. 1254–1266. doi: 10.1049/iet-cta.2017.0898.
- Oldham, K. B. and Spanier, J. (1974) *The fractional calculus: theory and applications of differentiation and integration to arbitrary order*. Academic Press.
- Phung, S. L. and Bouzerdoum, A. (2007) 'A new image feature for fast detection of people in images', *International Journal of Information and Systems Sciences*, 3(3), pp. 383–391.

- Qing, C. (2012) 'A fractional differential approach to low contrast image enhancement', *Int J Knowl Lang Process*, 3(2), pp. 20–29.
- Ren, H. et al., (2010) 'Fast object detection using boosted co-occurrence histograms of oriented gradients', *2010 IEEE International Conference on Image Processing*. IEEE.
- Rodrigues, M. T. A. et al., (2014) 'Evaluating cluster detection algorithms and feature extraction techniques in automatic classification of fish species', *Pattern Analysis and Applications*. Springer Nature, 18(4), pp. 783–797.
- Ross, B. (ed.) (1975) *Fractional Calculus and Its Applications*. Berlin, Heidelberg: Springer Berlin Heidelberg (Lecture Notes in Mathematics).
- Sabatier, J., Agrawal, O. P. and Machado, J. A. T. (2007) *Advances in fractional calculus: theoretical developments and applications in physics and engineering*. Springer Verlag.
- Sabzmeydani, P. and Mori, G. (2007) 'Detecting Pedestrians by Learning Shapelet Features', *IEEE Conference on Computer Vision and Pattern Recognition*. IEEE.
- Senechal, T., Bailly, K. and Prevost, L. (2012) 'Impact of action unit detection in automatic emotion recognition', *Pattern Analysis and Applications*. Springer Nature, 17(1), pp. 51–67. doi: 10.1007/s10044-012-0279-5.
- Shannon, C. E. (1949) *The Mathematical Theory of Communication*. By CE Shannon and Warren Weaver. Urbana.
- Sundaram, S. and Ramakrishnan, A. G. (2013) 'Performance enhancement of online handwritten Tamil symbol recognition with reevaluation techniques', *Pattern Analysis and Applications*. Springer Nature, 17(3), pp. 587–609. doi: 10.1007/s10044-013-0353-7.
- Talu, M. F. et al., (2013) 'Calculation of melatonin and resveratrol effects on steatosis hepatis using soft computing methods', *Computer Methods and Programs in Biomedicine*, 111(2). doi: 10.1016/j.cmpb.2013.04.020.
- Tian, D., Wu, J. F. and Yang, Y. J. (2013) 'A Fractional-order Sobel Operator for Medical Image Structure Feature Extraction', *Advanced Materials Research*. Trans Tech Publications, 860–863, pp. 2910–2913.
- Tian, D., Wu, J. and Yang, Y. (2014) 'A fractional-order edge detection operator for medical image structure feature extraction', *The 26th Chinese Control and Decision Conference (CCDC)*. IEEE.
- Wang, X. and Paliwal, K. K. (2003) 'Feature extraction and dimensionality reduction algorithms and their applications in vowel recognition', *Pattern Recognition*. Elsevier BV, 36(10), pp. 2429–2439.
- Watanabe, T., Ito, S. and Yokoi, K. (2009) 'Co-occurrence Histograms of Oriented Gradients for Pedestrian Detection', *Advances in Image and Video Technology*. Springer Berlin Heidelberg, pp. 37–47.
- Xiang, Y. et al., (2018) 'A SVR–ANN combined model based on ensemble EMD for rainfall prediction', *Applied Soft Computing*. Elsevier, 73, pp. 874–883.
- Xu, J. et al., (2012) 'Object Detection Based on Co-occurrence GMuLBP Features', *IEEE International Conference on Multimedia and Expo*. IEEE.
- Yang, Z. et al., (2011) 'The construction of fractional differential gradient operator', *Journal of Computational Information Systems*, 7(12), pp. 4328–4342.
- Zarei, J. and Tabatabaei, M. (2018) 'Fractional order unknown input filter design for fault detection of discrete fractional order linear systems', *Transactions of the Institute of Measurement and Control*, 40(16), pp. 4321–4329.